

## Antimicrobial and mosquito larvicidal activity of iron oxide nanoparticles phytosynthesized from the medicinal plant *Andrographis serpyllifolia*

Venkatachalam SOUNDARYA, Natchimuthu KARMEGAM\*

PG and Research Department of Botany, Government Arts College (Autonomous), Salem, 636 007, Tamil Nadu, India;  
[soundaryavenkatachalam4@gmail.com](mailto:soundaryavenkatachalam4@gmail.com); [kanishkarmegam@gmail.com](mailto:kanishkarmegam@gmail.com) (\*corresponding author)

### Abstract

Nanoparticles (NPs) play a significant role in protecting human and environmental health. Worldwide, research is focused on developing new pharmaceuticals and environmentally safe materials. The current research reports the phytosynthesis of NPs from iron oxide ( $\text{Fe}_2\text{O}_3$ ) mediated through ethanolic extracts of *Andrographis serpyllifolia* leaf (ASL) and their antimicrobial (bacteria and fungi) and mosquito (*Culex quinquefasciatus*) larvicidal activity. ASL was treated with aqueous iron chloride solution to turn into synthesized  $\text{Fe}_2\text{O}_3$ -NPs. The biosynthesized ASL- $\text{Fe}_2\text{O}_3$ -NPs were characterized with spectroscopic, electron microscopic and X-ray analyses. The synthesized ASL- $\text{Fe}_2\text{O}_3$ -NPs were characteristically showed triclinic crystal shape in SEM. The purity of synthesized  $\text{Fe}_2\text{O}_3$  nanoparticles was confirmed by FT-IR analysis. Out of twelve different selective pathogens (4 G<sup>+</sup>ve bacteria, 4 G<sup>-</sup>ve bacteria and 4 fungal species) tested with ASL- $\text{Fe}_2\text{O}_3$ -NPs, a maximum of 20.3 mm inhibition zone against *Staphylococcus aureus* among G<sup>+</sup>ve bacteria and 19.1 mm inhibition zone against *Pseudomonas aeruginosa* among G<sup>-</sup>ve bacteria was observed; while it was 16.9 mm against fungi (*Aspergillus niger*) at a test concentration of 100  $\mu\text{L}$ . The exposure of 4<sup>th</sup> instar larvae for 48 h to ASL- $\text{Fe}_2\text{O}_3$ -NPs exhibited a significant LC<sub>50</sub> value at 12.80 ppm. The study findings reveal that the  $\text{Fe}_2\text{O}_3$ -NPs synthesized using *A. serpyllifolia* leaf extract could be a potential source for antibacterial, antifungal and mosquito larvicidal activities.

**Keywords:** bactericidal activity; biogenic nanoparticles; *Culex quinquefasciatus*;  $\text{Fe}_2\text{O}_3$  nanoparticles; microbial inhibition

### Introduction

With the advancement of modern technology, nanotechnology has been gaining a lot of success *via* greener, safer, cheaper, and biologically acceptable methods of synthesis (Priya *et al.*, 2021). Among various metallic nanoparticles (NPs), iron oxide ( $\text{Fe}_2\text{O}_3$ ) NPs have numerous applications such as therapeutics, drug delivery, biomedicines and cancer treatment agents (Qasim *et al.*, 2020).  $\text{Fe}_2\text{O}_3$  NPs can be synthesized using a variety of chemical and physical methods. The starting materials and energy used in these methods are potentially hazardous.  $\text{Fe}_2\text{O}_3$  nanostructures with low dimensions remain a challenge to synthesize in a simple

Received: 17 Aug 2023. Received in revised form: 26 Sep 2023. Accepted: 13 Nov 2023. Published online: 23 Nov 2023.

From Volume 13, Issue 1, 2021, Notulae Scientia Biologicae journal uses article numbers in place of the traditional method of continuous pagination through the volume. The journal will continue to appear quarterly, as before, with four annual numbers.

and reliable manner. Nanotechnology has the primary purpose of developing eco-friendly ways to synthesize nanoparticles (Balamurugan *et al.*, 2014). Medically, the pathogenic microorganisms and the insect vectors like mosquitoes are undying problems requiring effective mitigation. It is possible for pathogenic bacteria to develop drug resistance, while mosquitoes transmit deadly diseases, posing a threat to human health. Phytosynthesized NPs exert enhanced stability, antimicrobial and antilarval activities due to their surface properties that can be developed and used for diverse applications (Lourthuraj *et al.*, 2020; Balachandar *et al.*, 2022; Calabrese *et al.*, 2022).

*Andrographis serpyllifolia* (Vahl.) Wight is a prostrate herb which belongs to the family Acanthaceae. It is an endemic medicinal herb found in wild. Traditional Indian medicine uses parts of *A. serpyllifolia* to remove ticks from cattle. This plant can be used to treat fever, wounds, and jaundice with its root extract and extract from the leaves (Alagesabooopathi, 2000). *A. serpyllifolia* leaf extracts have shown anti-venom activities against toxic venom enzymes of snakes *in vitro* (Balu and Alagesabooopathi, 1995; Hansiya and Geetha, 2021). The chemical investigation of *A. serpyllifolia* revealed the presence of serpyllin, a new flavone (Govindachari *et al.*, 1968). Alkaloids, tannins, terpenoids, steroids, flavonoids and polyphenol compounds are the phytochemicals known in *A. serpyllifolia* by qualitative analysis (Deepa *et al.*, 2013). *A. serpyllifolia* contain many important phytochemicals, which can act as capping agents in NPs synthesis and reveals the antimicrobial properties. Silver (Ag) NPs from *A. serpyllifolia* are reported to possess antimicrobial, antifungal, biocompatibility, anti-inflammatory, anticancer, antioxidant and larvicidal activities (Stephen and Thomas, 2020).

Green synthesis is the field of nanobiotechnology which has wide range of applications including phytosynthesized NPs for medical utility. Antibacterial and larvicidal activity was revealed by synthesized Ag NPs using *A. serpyllifolia* leaf extract (Madhankumar *et al.*, 2019). However, phytosynthesis of Fe<sub>2</sub>O<sub>3</sub>-NPs with *A. serpyllifolia* leaf extract and their antibacterial, antifungal and mosquito larvicidal activity has not been addressed. As the activity of phytosynthesized Fe<sub>2</sub>O<sub>3</sub>-NPs are highly effective and advantageous (Haseena *et al.*, 2021), its' exploration is occupying a significant role in biomedical applications. Hence, the present study has been carried out to phytosynthesize Fe<sub>2</sub>O<sub>3</sub>-NPs using ethanolic leaf extract, characterize them and to test the NPs against selective bacteria, and fungi by *in vitro* assay using well diffusion method in addition to larvicidal assay against 4<sup>th</sup> instar larvae of *Culex quinquefasciatus* mosquito.

## Materials and Methods

### *Collection and processing of Andrographis serpyllifolia leaves*

The medicinal plant, *A. serpyllifolia* of Acanthaceae (Figure 1) was collected from Kanjamalai Hills (J2CM+H65: Lat. – 11.621403°, Long. – 78.033257°), Salem (Southern Eastern Ghats), and identified with the help of local floras and confirmed the identification with the taxonomist, Dr. S. Karuppusamy, Madura College, Madurai. *A. serpyllifolia* leaves (ASL) were collected and shade dried for a week and subjected to extraction with ethyl alcohol (AR grade).

### *Synthesis and characterization of Fe<sub>2</sub>O<sub>3</sub> nanoparticles*

The ASL solution was prepared according to the procedure of Haseena *et al.* (2020). Accurately, 10 mL of ASL extract was slowly blended with FeCl<sub>3</sub> (20 mL of 1 M) and subjected to annealing at 80 °C through uninterrupted magnetic stirring for 10 mins. The formation of Fe<sub>2</sub>O<sub>3</sub>-NPs was confirmed by the appearance of brownish-red color. Repeated washing of the prepared Fe<sub>2</sub>O<sub>3</sub>-NPs was done by centrifugation to exclude the contaminants before drying for further investigations. The prepared Fe<sub>2</sub>O<sub>3</sub>-NPs were subjected to UV-Visible spectroscopic analysis (Shimadu-1800, China), Fourier Transform Infra-red Spectroscopy (FT-IR, Perkin Elmer), and powder X-ray diffraction (XRD) pattern (Rigaku Miniflex-II diffractometer). The surface of the

ASL-Fe<sub>2</sub>O<sub>3</sub>-NPs was observed with an electron microscope (SEM, ZEISS EVO) while the elemental composition was determined using an EDX spectrometer.

*Test microorganisms and antimicrobial activity*

Each four species of G<sup>+</sup>ve and G<sup>-</sup>ve bacteria along with four fungal species were used in the study (*Staphylococcus aureus*, *Bacillus subtilis*, *Enterococcus faecalis*, *Micrococcus luteus*, *Escherichia coli*, *Salmonella typhi*, *Klebsiella pneumoniae*, *Pseudomonas aeruginosa*, *Aspergillus niger*, *Candida albicans*, *Candida tropicalis* and *Candida glabrata*). The bacterial (Muller Hinton Agar medium) and fungal test (Potato Dextrose Agar medium) organisms were subjected to antimicrobial assay with well diffusion method using standard antibiotics (positive control), 25, 50, 75 and 100 µL/mL concentration of ASL-Fe<sub>2</sub>O<sub>3</sub>-NPs. The standard antibiotics (20 µg) used were chloramphenicol and fluconazole for bacteria and fungi, respectively. The streaked triplicate Petri dishes per treatment were placed in an incubator at 37 °C and observed for growth after every 24 h. The results obtained were recorded and expressed as mean of three replicates ± standard deviation.

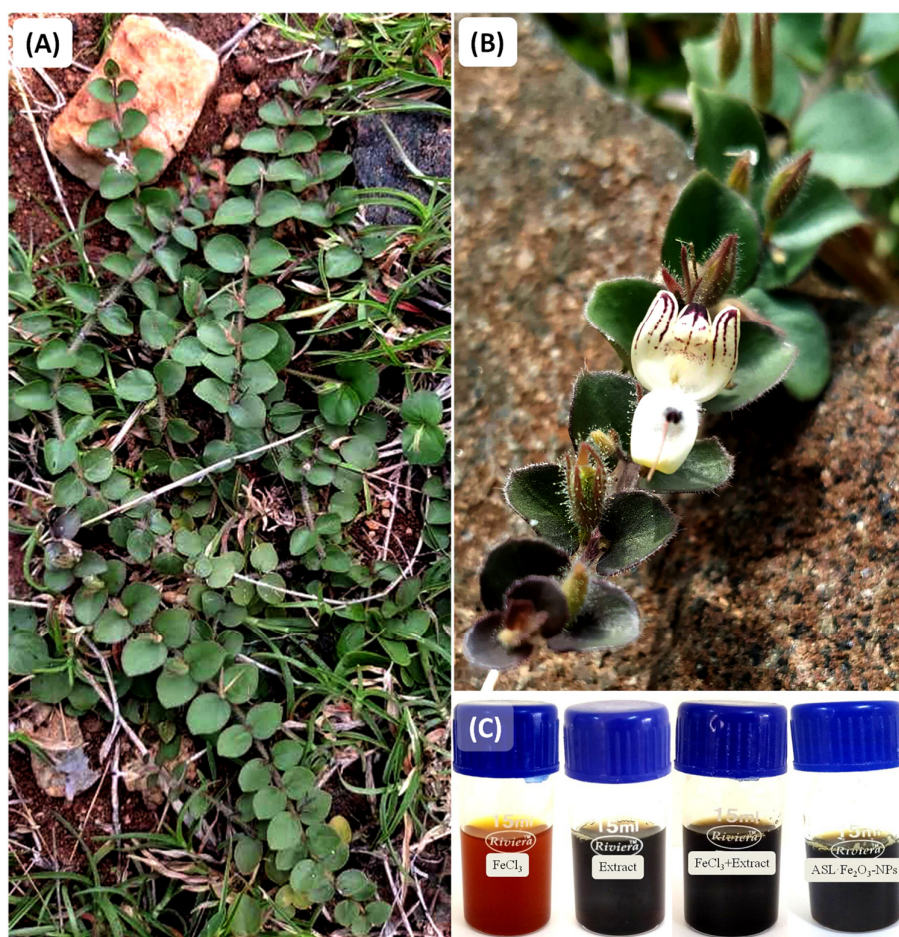


**Figure 1.** *A. serpyllifolia* (A) Habit; (B) Flowering branch; (C) Phytosynthesis of Fe<sub>2</sub>O<sub>3</sub> NPs

*Mosquito larvicidal bioassay*

Mosquito larvae (*Culex quinquefasciatus*) of F3 generation (4<sup>th</sup> instar) laboratory-cultures were experimented with 1, 5, and 10 ppm concentrations of ASL-Fe<sub>2</sub>O<sub>3</sub>-NPs. The treatment containing DD water excluding NPs was also maintained (control). All the treatments were replicated five times in 250 mL glass beakers each with 100 mL DD water and 25 number of 4<sup>th</sup> instar larvae. The treatments were maintained as

per the procedure adopted by Karmegam *et al.* (1997). The percentage of dead larvae in all the treatments was observed after 24 h and 48 h. With the obtained results, percentage larval mortality was calculated and subjected to Finney's Probit analysis.

## Results and Discussion

### *Evaluation of ASL-Fe<sub>2</sub>O<sub>3</sub>-NPs*

UV-Visible spectroscopy is the mostly used technique for the observation of NPs synthesis. Appearance of reddish brown colored solution after the iron chloride was treated with plant extract is characteristics of Fe<sub>2</sub>O<sub>3</sub>-NPs. UV-Vis spectroscopy showed the absorption spectra of Fe<sub>2</sub>O<sub>3</sub>-NPs disintegrated in DD water presented a broad absorption peak ( $\approx 210$  nm) and a curve at 300 nm wavelength range which specified the characteristics of the biogenic ASL-Fe<sub>2</sub>O<sub>3</sub>-NPs (Figure 2A). In previous research, Fe<sub>2</sub>O<sub>3</sub>-NPs from garlic and onion peel extracts showed the high transmittance spectra of 200 to 400 nm, which matches with the present research (Abid *et al.*, 2021). The UV-Vis spectra for synthesized ASL-Fe<sub>2</sub>O<sub>3</sub>-NPs showed the characteristic 406 nm peak and 3.05 eV band gap (Kirdat *et al.*, 2021). The green synthesis of Fe<sub>2</sub>O<sub>3</sub>-NPs with *Withania coagulans* was confirmed by sharp UV-Vis spectral peaks at 294 nm and 278 nm (Qasim *et al.*, 2020). The UV-Vis spectra of Fe<sub>3</sub>O<sub>4</sub>-NPs have absorption peaks at 240 nm and 402 nm which denotes the genesis of Fe<sub>2</sub>O<sub>3</sub>-NPs (Patil *et al.*, 2020). The color changes from yellow to black during the development of Fe<sub>2</sub>O<sub>3</sub>-NPs. The maximum absorption appeared at 300 nm of Fe<sub>2</sub>O<sub>3</sub> NPs due to the vibration of the band of Fe<sub>2</sub>O<sub>3</sub>-NPs. The absorption band at a wavelength of 275-400 nm indicates the Fe<sub>2</sub>O<sub>3</sub>-NPs formation (Dildar *et al.*, 2021).

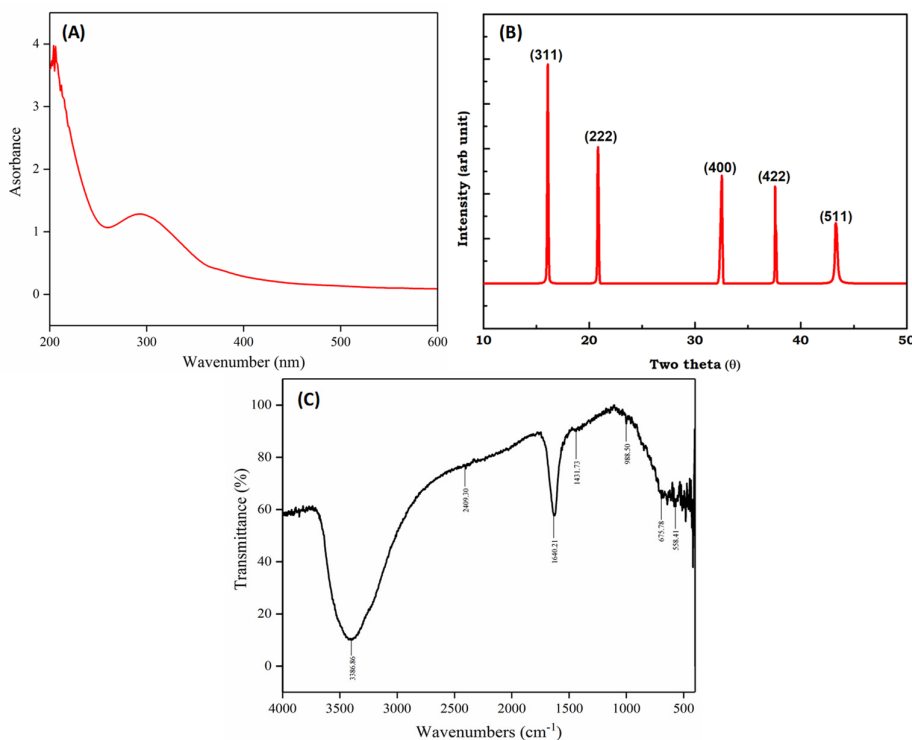


**Figure 2.** Characterization of ASL-Fe<sub>2</sub>O<sub>3</sub>-NPs using (A) UV-Vis spectroscopy, (B) XRD and (C) FT-IR

X-ray diffraction analysis was carried out for determining the size of synthesized ASL-Fe<sub>2</sub>O<sub>3</sub>-NPs by Debye–Scherrer equation ( $D = 0.9\lambda / \beta \cos \theta$ ) and to study the structure, and crystallinity of the synthesized Fe<sub>2</sub>O<sub>3</sub> NPs. For the developed ASL-Fe<sub>2</sub>O<sub>3</sub>-NPs, the diffraction angle was 15.2° (311), 21.5° (222), 32.8° (400), 37.5° (422), 43.2° (511). The size of the ASL-Fe<sub>2</sub>O<sub>3</sub>-NPs was from the highest peak (5.10° nm) with a 2θ value of 15.2° and with (311) plane (Figure 2B).

*Mikania mikrantha* leaf extract in XRD analysis showed 30.27° (220), 35.60° (311), 36.75° (222), 43.41° (400), 53.88° (422), 57.38° (511) and 62.90° (440) which provides crystalline form of NPs and its size was 20.27 nm according to Debye – Scherrer equation (Biswas *et al.*, 2021). *Canthium coromandelicum* leaf extract showed the XRD pattern at 2 θ values 30.11° (116), 35.21° (206), 43.22° (226), 56.21° (406). The average crystalline size of Fe<sub>2</sub>O<sub>3</sub> NPs calculated using Debye–Scherrer equation and it was found at 19.25 nm (Sudhakar *et al.*, 2021). The crystal structure and Fe<sub>2</sub>O<sub>3</sub>-NPs size were ascertained using XRD analysis, where narrow peaks indicate more crystalline structure and broad peaks reveal that they are more functional and efficient at 47° (311), 54° (400), 60° (422), 73° (440), 68° (511) and 77° (553) planes of crystal lattice (Qasim *et al.*, 2020). It has been reported that the synthesized Fe<sub>2</sub>O<sub>3</sub> NPs showed the peak at 311 plane, which is matching with the standard Fe<sub>2</sub>O<sub>3</sub>-NPs with the peaks at 17.19° (111), 29.01° (310), 31.31° (311), and 34.91° (320) (Patil *et al.*, 2020).

The FT-IR analysis ASL-Fe<sub>2</sub>O<sub>3</sub>-NPs in the present study showed a wavenumber range of 500–4000 cm<sup>-1</sup>. The FT-IR spectrum of the ASL-Fe<sub>2</sub>O<sub>3</sub>-NPs exhibited peaks at 558.41, 675.78, 988.50, 1431.73, 1640.21, 2409.30, and 3386.86 cm<sup>-1</sup>. The distinct peaks appeared at 558.41 and 675.78 cm<sup>-1</sup> as a consequence of inherent vibrational expansion of oxygen bond reveal that the developed NPs were Fe<sub>2</sub>O<sub>3</sub>. The small peak appeared in 988 cm<sup>-1</sup> was due to nitrate group. The occurrence of 1640.21 and 3386.86 cm<sup>-1</sup> absorption peaks specifies the surface hydroxyl groups. The FT-IR analysis thus validates the synthesized NPs were Fe<sub>2</sub>O<sub>3</sub> without impurities (Figure 2C). Similarly, in the biogenically synthesized Fe<sub>2</sub>O<sub>3</sub>-NPs of ginger extract showed the FT-IR spectra between 500 and 4000 cm<sup>-1</sup> where the expansion at 536.11 cm<sup>-1</sup> represents Fe-O vibration. The small vibration at 1635.34 cm<sup>-1</sup> indicates the presence of alkaline group. The peaks at 3455.81 and 3428.81 cm<sup>-1</sup> represent O-H bonds, whereas 2921.63 cm<sup>-1</sup> peak indicates C-H bonds (Kirdat *et al.*, 2021). In *M. micrantha*, Fe<sub>3</sub>O<sub>4</sub>-NPs displayed the absorption bands at 3302 and 3317 cm<sup>-1</sup> because of extended vibrations of O-H bunch in alcoholic and phenolic blends; while the normal absorption bands at 1641 and 1636 cm<sup>-1</sup> are representing amides I and II, respectively. In Fe<sub>2</sub>O<sub>3</sub>-NPs synthesized using *W. coagulans* extract, the FT-IR spectral range observed was 657, 666, 1044, 1593, 2351, and 2954 cm<sup>-1</sup>. The appearance of 666 and 657 cm<sup>-1</sup> peaks correspond to the vibration of oxygen bond. The synthesized Fe<sub>2</sub>O<sub>3</sub>-NPs showed absorption peak at 1044 cm<sup>-1</sup> (Qasim *et al.*, 2020). The stretching vibrations at 3392.79 cm<sup>-1</sup> indicates the OH groups, while 600 cm<sup>-1</sup> is O-Fe bonds stretching (Dildar *et al.*, 2021).

The SEM images of ASL-Fe<sub>2</sub>O<sub>3</sub>-NPs revealed the average particle size of 20.11 nm with the stabilized triclinic crystal-like structure (Figure 3A-B). Similarly, *M. mikrantha* leaf extract derived NPs showed similar structures to that of nanosheet frames with a particle size range of 24–44 nm (Biswas *et al.*, 2021). The biogenic synthesized *C. coromandelicum* leaf extract revealed the morphology which is not uniform but in spherical form (Sudhakar *et al.*, 2021). The synthesized Fe<sub>2</sub>O<sub>3</sub>-NPs showed agglomeration of irregular clusters (Qasim *et al.*, 2020). The confirmation of Fe<sub>2</sub>O<sub>3</sub>-NPs by SEM analysis which is granular and spherical in shape (Patil *et al.*, 2020). ASL-Fe<sub>2</sub>O<sub>3</sub>-NPs, stabilize the phyto-capping agents. Irregular morphologies was observed in the synthesized Fe<sub>2</sub>O<sub>3</sub>-NPs from guava extract (Dildar *et al.*, 2021).

In the present study, EDX spectra were used to reveal the purity of synthesized ASL-Fe<sub>2</sub>O<sub>3</sub>-NPs (Figure 3C). Iron, oxygen and chlorine obtained in EDX spectra were confirmed. The presence of chlorine content could be attributed to the biomolecules in *A. serpyllifolia* leaf extract binding to the surface of ASL-Fe<sub>2</sub>O<sub>3</sub>-NPs. The weight percentage of 52.30, 35.97 and 11.72 was obtained for oxygen, chlorine and iron respectively in the present study which showed variations in different plant derived NPs. For instance, the fruit peel powder of

pomegranate displayed 77.14 wt % of carbon and 22.86 wt% of oxygen (Yusefi *et al.*, 2020). In *Carica papaya* leaf extract, 25.05% carbon, 31.03% oxygen and 32.70% iron was found where the carbon is represented as impurities found in Fe<sub>2</sub>O<sub>3</sub> NPs (Bhuiyan *et al.*, 2020). The total weight percentage of 31.41 for iron, and 24.86 for oxygen observed along with some impurities like chlorine with 40.2% of total percentage were present in the composition of *W. coagulans* derived Fe<sub>2</sub>O<sub>3</sub>-NPs (Qasim *et al.*, 2020).

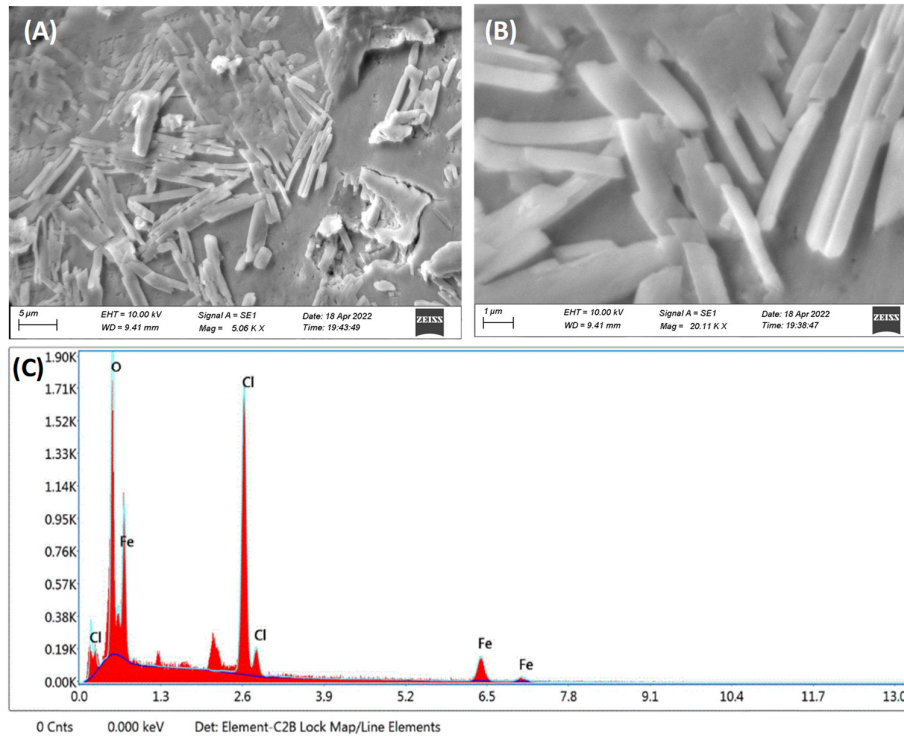


**Figure 3.** FE-SEM images (A, B) and EDX spectrum of ASL-Fe<sub>2</sub>O<sub>3</sub>-NPs

#### *Antimicrobial activity of biosynthesized ASL-Fe<sub>2</sub>O<sub>3</sub>-NPs*

ASL-Fe<sub>2</sub>O<sub>3</sub>-NPs exhibited considerable antibacterial activity against G<sup>+</sup> and G<sup>-</sup> bacteria with the higher zone of inhibition (ZOI). A maximum of 20.3 mm ZOI was observed against *S. aureus*, followed by *E. faecalis* (19.0 mm ZOI), *M. luteus* (18.2 mm ZOI) and *B. subtilis* (17.1 mm ZOI). ASL-Fe<sub>2</sub>O<sub>3</sub> NPs recorded the ZOI of 18.0, 14.9 and 17.4 mm against *E. coli*, *K. pneumoniae* and *S. typhi*, respectively. Among the G<sup>-</sup> bacteria tested, the highest ZOI of 19.1 mm at 100 μL/mL concentration was found against *P. aeruginosa* while the lower concentrations expressed lesser activity (Figure 4 and Figure 5).

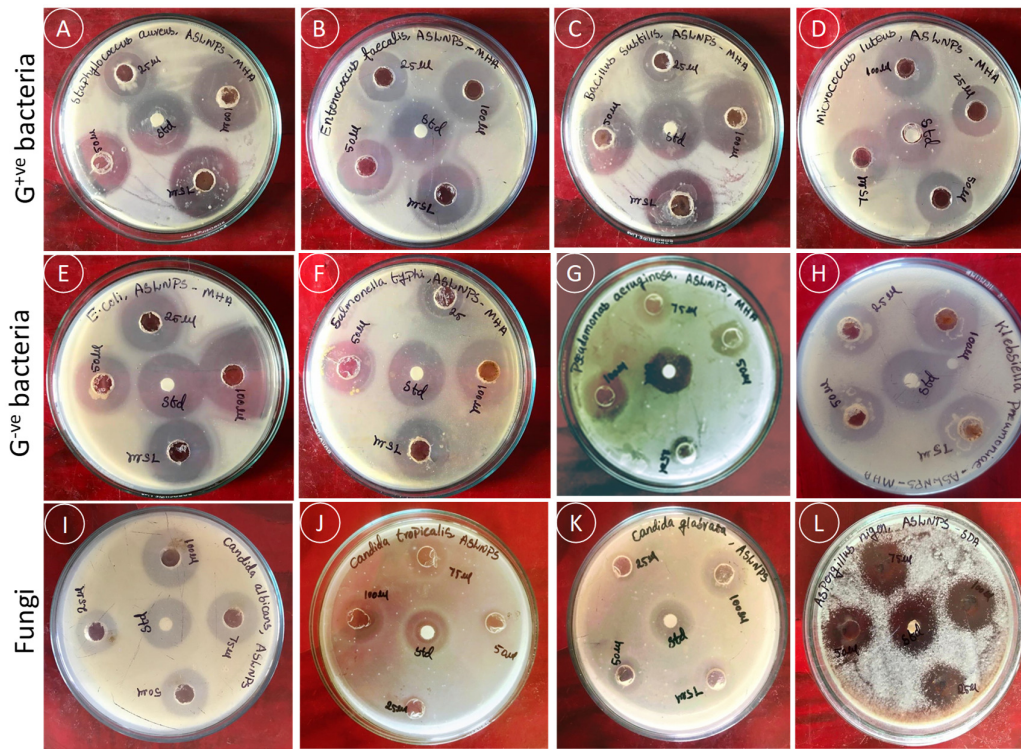


**Figure 4.** Antibacterial and antifungal activities of ASL-Fe<sub>2</sub>O<sub>3</sub>-NPs (A = *S. aureus*, B = *B. subtilis*, C = *E. faecalis*, D = *M. luteus*, E = *E. coli*, F = *S. typhi*, G = *K. pneumoniae*, H = *P. aeruginosa*, I = *A. niger*, J = *C. albicans*, K = *C. tropicalis* and L = *C. glabrata*)

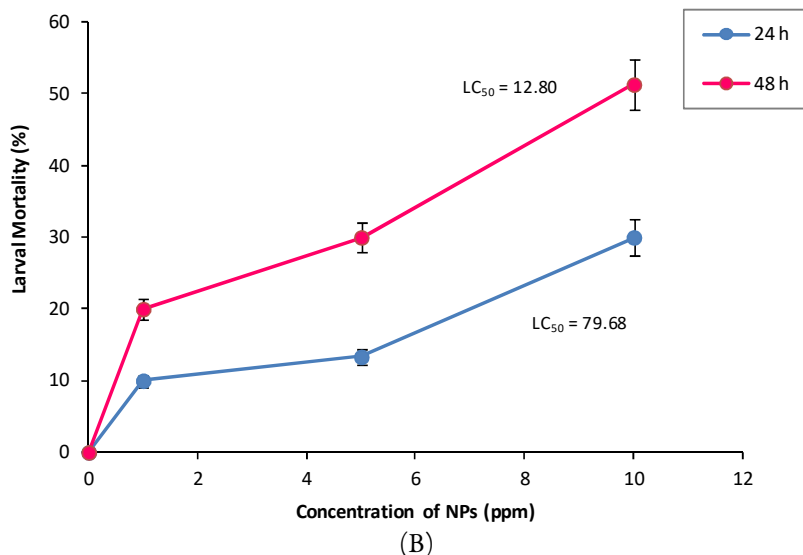
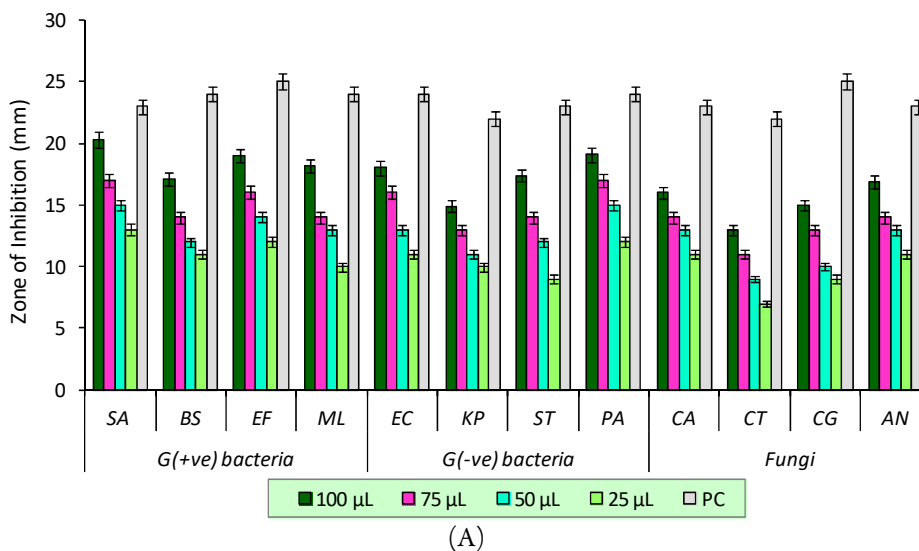


**Figure 5.** (A) Zone of inhibition by test microorganisms to ASL-Fe<sub>2</sub>O<sub>3</sub>-NPs (Values are mean of triplicates ± std. deviation; SA = *S. aureus*, BS = *B. subtilis*, EF = *E. faecalis*, ML = *M. luteus*, EC = *E. coli*, ST = *S. typhi*, KP = *K. pneumoniae*, PA = *P. aeruginosa*, AN = *A. niger*, CA = *C. albicans*, CT = *C. tropicalis* and CG = *C. glabrata*; PC = Positive control); (B) Mosquito larvicidal activity of ASL-Fe<sub>2</sub>O<sub>3</sub>-NPs against 4<sup>th</sup> instar larvae of *C. quinquefasciatus* (Values are mean of three replicates ± std. deviation)

Green synthesized Fe<sub>2</sub>O<sub>3</sub>-NPs using *W. coagulans* showed effective antibacterial activity against *S. aureus* while it was less effective against *P. aeruginosa* (Qasim *et al.*, 2020). The antibacterial activity in *C. coromandelicum* leaf extract derived Fe<sub>2</sub>O<sub>3</sub>-NPs expressed the highest ZOI against the G<sup>+</sup> *S. aureus* and the G<sup>-</sup> *S. typhi* (Sudhakar *et al.*, 2021). The Fe<sub>2</sub>O<sub>3</sub> NPs illustrated a maximum ZOI against *S. aureus* while no activity against *Bacillus pumilus* (Dildar *et al.*, 2021). The antibacterial activity in *Andrographis paniculata* expressed a significant ZOI against *S. aureus* whereas lowest ZOI was observed against *K. pneumoniae* (Bhuiyan *et al.*, 2020) which is corroborating with that of the present study findings. Depending on the nature of plant material, the Fe<sub>2</sub>O<sub>3</sub>-NPs demonstrate fluctuation in antibacterial activity. This is a clear evidence that can be seen by comparing the previous studies with Fe<sub>2</sub>O<sub>3</sub>-NPs which showed the highest ZOI against *S. aureus*

(Bhuiyan *et al.*, 2020; Dildar *et al.*, 2021; Qasim *et al.*, 2020; Sudhakar *et al.*, 2021) and lowest ZOI against *K. pneumoniae* (Bhuiyan *et al.*, 2020) similar to that of the present study. Significant antimicrobial activity against fungi by ASL-Fe<sub>2</sub>O<sub>3</sub>-NPs was observed with a ZOI of 16.0 mm against *C. albicans* followed by *C. glabrata* (15.4 mm ZOI) and *C. tropicalis* (12.8 mm ZOI) whilst *A. niger* displayed the highest ZOI of 16.9 mm at 100 µL concentration (Figure 4 and Figure 5A). *M. mikrantha* leaf extract derived Fe<sub>2</sub>O<sub>3</sub>-NPs indicated high antifungal activity against *C. albicans* (Bhuiyan *et al.*, 2020), where the ZOI is higher than the present study.

#### *Mosquito larvicidal activity of ASL-Fe<sub>2</sub>O<sub>3</sub>-NPs*

The mosquito larvae (4<sup>th</sup> instar) exposed to different concentrations of ASL-Fe<sub>2</sub>O<sub>3</sub>-NPs exhibited concentration-dependent mortality, while 42 h exposure resulted in higher mortality than 24 h exposure (Figure 5B). There has been a high degree of dose-dependent and exposure-time-dependent larvicidal activity against the vector mosquitoes, *Anopheles stephensi* and *Aedes aegypti* reported in a similar study which employed Fe<sub>2</sub>O<sub>3</sub>-NPs biosynthesized with the leaf extract of *Grivillea robusta* (Zargham *et al.*, 2023). A maximum of 51.33% larval mortality was observed in 10 ppm ASL-Fe<sub>2</sub>O<sub>3</sub>-NPs after 48 h was recorded with a highly significant Chi-square values. The LC<sub>50</sub> values for 24 h and 42 h respectively were 79.68 and 12.80 ppm against 4<sup>th</sup> instar larvae of *C. quinquefasciatus*. In a similar study, Madhankumar *et al.* (2019) reported much higher LC<sub>50</sub> (68.889 ppm) concentrations of AgNPs phytosynthesized from the leaves of *A. serpyllifolia*. In comparison, the larvicidal activity of ASL-Fe<sub>2</sub>O<sub>3</sub>-NPs in the present study was much more pronounced indicating that Fe<sub>2</sub>O<sub>3</sub>-NPs obtained from *A. serpyllifolia* is efficacious. Phytochemical components present in plants are responsible for the formation of biologically active nanomaterials. It is possible to create mosquito larvicidal properties in metallic nanoparticles using the phytochemicals of the raw natural materials (Li *et al.*, 2023).

## Conclusions

Phytosynthesis of Fe<sub>2</sub>O<sub>3</sub>-NPs mediated through *A. serpyllifolia* leaf extract was demonstrated. Synthesized ASL-Fe<sub>2</sub>O<sub>3</sub>-NPs' characterization with UV-Vis, FT-IR, XRD, SEM and EDX analyses confirmed the formation of biogenic Fe<sub>2</sub>O<sub>3</sub>-NPs. ASL-Fe<sub>2</sub>O<sub>3</sub>-NPs presented good antimicrobial activity against selective microorganisms. The highest ZOI of 20.3 mm was observed against *S. aureus* amongst G<sup>+ve</sup> bacteria, while *P. aeruginosa* exhibited the highest ZOI of 19.1 mm amongst G<sup>-ve</sup> bacteria. The antifungal activity of ASL-Fe<sub>2</sub>O<sub>3</sub> NPs revealed the highest ZOI of 16.9 mm against *A. niger*. A lowest LC<sub>50</sub> concentration of 12.80 ppm ASL-Fe<sub>2</sub>O<sub>3</sub>-NPs in 48 h bioassay study was recorded in the current study against mosquito larvae. Thus the phytosynthesized ASL-Fe<sub>2</sub>O<sub>3</sub>-NPs could be developed into effective antimicrobial and mosquito larvicidal agent.

## Authors' Contributions

VS: Investigation, data collection and manuscript writing, interpretation; NK: Conceptualization, supervision, study design, review and editing of final manuscript and correction.

All authors read and approved the final manuscript.

### **Ethical approval** (for researches involving animals or humans)

Not applicable.

### **Acknowledgements**

This work was supported by Tamil Nadu State Council for Science and Technology (TNSCST), Chennai, in the form of Student Project Scheme (Grant number: TNSCST/SPS/2021-2022, BS-554).

### **Conflict of Interests**

The authors declare that there are no conflicts of interest related to this article.

### **References**

- Abid MA, Abid DA, Aziz WJ, Rashid TM (2021). Iron oxide nanoparticles synthesized using garlic and onion peel extracts rapidly degrade methylene blue dye. *Journal of Physics: Condensed Matter* 622:413277. <https://doi.org/10.1016/j.physb.2021.413277>
- Alagesabopathi C (2000). *Andrographis* spp.: A source of bitter compounds for medicinal use. *Ancient Science of Life* 19:164-168.
- Balachandar R, Navaneethan R, Biruntha M, Krishna Kumar A, Govarthanan M, Karmegam N (2022). Antibacterial activity of silver nanoparticles phytosynthesized from *Glochidion candolleianum* leaves. *Materials Letters* 311:131572. <https://doi.org/10.1016/j.matlet.2021.131572>
- Balamurugan M, Saravanan S, Soga T (2014). Synthesis of iron oxide nanoparticles by using *Eucalyptus globulus* plant extract. *e-Journal Surface Science and Nanotechnology* 12:363-367. <https://doi.org/10.1380/ejsnt.2014.363>
- Balu S, Alagesabopathi C (1995). Antivenom activities of some species of *Andrographis* Wall. *Ancient Science of Life* 14:187-190.
- Bhuiyan MHS, Miah MY, Paul SC, Aka TD, Saha O, Rahaman MM, Sharif MJI, Habiba O, Ashaduzzaman M (2020). Green synthesis of iron oxide nanoparticle using *Carica papaya* leaf extract: application for photocatalytic degradation of remazol yellow RR dye and antibacterial activity. *Heliyon* 6:e04603. <https://doi.org/10.1016/j.heliyon.2020.e04603>
- Biswas A, Vanlalveni C, Lalfakzuala R, Soumitra Nath, Rokhum L (2021). *Mikania mikrantha* leaf extract mediated biogenic synthesis of magnetic iron oxide nanoparticles: Characterization and its antimicrobial activity study. *Materials Today: Proceedings* 42:1366-1373.
- Calabrese C, La Parola V, Testa ML, Liotta LF (2022). Antifouling and antimicrobial activity of Ag, Cu and Fe nanoparticles supported on silica and titania. *Inorganica Chimica Acta* 529:120636. <https://doi.org/10.1016/J.ICA.2021.120636>
- Deepa S, Rajaram K, Suresh Kumar P (2013). *In vitro* and *in vivo* antidiabetic effect of *Andrographis lineata* Wall. Ex.Nees and *Andrographis serpyllifolia* Wt.Ic leaf extracts. *African Journal of Pharmacy and Pharmacology* 7:2112-2121. <https://doi.org/10.5897/AJPP2013.3655>
- Dildar N, Ali S, Sohail T, Lateef M, Khan S, Bukhari S, Fazil P (2021). Biosynthesis, characterization, radical scavenging and antimicrobial properties of *Psidium guajava* Linn coated silver and iron oxide nanoparticles. *Egyptian Journal of Chemistry* 65:145-152. <https://doi.org/10.21608/ejchem.2021.81802.4061>
- Govindachari TR, Parthasarathy PC, Pai BR, Kalyanaraman PS (1968). Chemical investigation of *Andrographis serpyllifolia*: Isolation and structure of serpyllin, a new flavone. *Tetrahedron* 24:7027-7031. [https://doi.org/10.1016/S0040-4020\(01\)96819-X](https://doi.org/10.1016/S0040-4020(01)96819-X)

- Hansiya VS, Geetha N (2021). *In vitro* anti-venom potential of various solvent based leaf extracts of *Andrographis serpyllifolia* (Rottler ex Vahl) Wight against *Naja naja* and *Daboia russelli*. Journal of Ethnopharmacology 269:113687. <https://doi.org/10.1016/j.jep.2020.113687>
- Haseena S, Shanavas S, Ahamad T, Alshehri SM, Baskaran P, Duraimurugan J, Acevedo R, Khan MAM, Anbarasan PM, Jayamani N (2021). Investigation on photocatalytic activity of bio-treated  $\alpha$ -Fe<sub>2</sub>O<sub>3</sub> nanoparticles using *Phyllanthus niruri* and *Moringa stenopetala* leaf extract against methylene blue and phenol molecules: Kinetics, mechanism and stability. Journal of Environmental Chemical Engineering 9(1):104996. <https://doi.org/10.1016/j.jece.2020.104996>
- Haseena S, Shanavas S, Duraimurugan J, Ahamad T, Alshehri SM, Acevedo R, Jayamani N (2020). Study on photocatalytic and antibacterial properties of phase pure Fe<sub>2</sub>O<sub>3</sub> nanostructures synthesized using *Caralluma fimbriata* and *Achyranthes aspera* leaves. Optik (Stuttgart) 203:164047. <https://doi.org/10.1016/j.ijleo.2019.164047>
- Karmegam N, Sakthivadivel M, Anuradha V, Daniel T (1997). Indigenous-plant extracts as larvicidal agents against *Culex quinquefasciatus* Say. Bioresource Technology 59:137-140. [https://doi.org/10.1016/S0960-8524\(96\)00157-5](https://doi.org/10.1016/S0960-8524(96)00157-5)
- Kirdat PN, Dandge PB, Hagwane RM, Nikam AS, Mahadik SP, Jirange ST (2021). Synthesis and characterization of ginger (*Z. officinale*) extract mediated iron oxide nanoparticles and its antibacterial activity. Materials Today: Proceedings 43:2826-2831. <https://doi.org/10.1016/j.matpr.2020.11.422>
- Li C, Han Y, Gao T, Zhang J, Xu DX, Wāng Y (2023). Insecticidal activity of metallic nanopesticides synthesized from natural resources: A review. Environmental Chemistry Letters 21(2):1141-1176. <https://doi.org/10.1007/s10311-022-01548-0>
- Lourthuraj AA, Selvam MM, Hussain MS, Abdel-Warith AWA, Younis EMI, Al-Asgah NA (2020). Dye degradation, antimicrobial and larvicidal activity of silver nanoparticles biosynthesized from *Cleistanthus collinus*. Saudi Journal of Biological Science 27:1753-1759. <https://doi.org/10.1016/j.sjbs.2020.05.008>
- Madhankumar R, Sivasankar P, Kalaimurugan D, Murugesan S (2019). Antibacterial and larvicidal activity of silver nanoparticles synthesized by the leaf extract of *Andrographis serpyllifolia* Wight. Journal of Cluster Science 31:719-726. <https://doi.org/10.1007/S10876-019-01679-5>
- Patil YY, Sutar VB, Tiwari AP (2020). Green synthesis of magnetic iron nanoparticles using medicinal plant *Tridax procumbens* leaf extracts and its application as an antimicrobial agent against *E. coli*. International Journal of Applied Pharmaceutics 12:34-39. <https://doi.org/10.22159/ijap.2020.v12s4.40102>
- Priya Naveen, Kaur K, Sidhu AK (2021). Green Synthesis: An eco-friendly route for the synthesis of iron oxide nanoparticles. Frontiers in Nanotechnology 3:655062. <https://doi.org/10.3389/fnano.2021.655062>
- Qasim S, Zafar A, Saif MS, Ali Z, Nazar M, Waqas M, Haq AU, Tariq T, Hassan SG, Iqbal F, Shu X-G, Hasan M (2020). Green synthesis of iron oxide nanorods using *Withania coagulans* extract improved photocatalytic degradation and antimicrobial activity. Journal of Photochemistry and Photobiology B: Biology 204:111784. <https://doi.org/10.1016/j.jphotobiol.2020.111784>
- Stephen S, Thomas T (2020). A review on green synthesis of silver nanoparticles by employing plants of Acanthaceae and its bioactivities. Nanomedicine Research Journal 5:215-224.
- Sudhakar C, Poonkothai M, Selvankumar T, Selvam K, Rajivgandhi G, Siddiqi MZ, Alharbi NS, Kadaikunnan S, Vijayakumar N (2021). Biomimetic synthesis of iron oxide nanoparticles using *Canthium coromandelicum* leaf extract and its antibacterial and catalytic degradation of Janus green. Inorganic Chemistry Communications 133:108977. <https://doi.org/10.1016/j.inoche.2021.108977>
- Yusefi M, Shameli K, Ali RR, Pang S-W, Teow S-Y (2020). Evaluating anticancer activity of plant-mediated synthesized iron oxide nanoparticles using *Punica granatum* fruit peel extract. Journal of Molecular Structure 1204:127539. <https://doi.org/10.1016/j.molstruc.2019.127539>
- Zargham F, Afzal M, Rasool K, Manzoor S, Qureshi NA (2023). Larvicidal activity of green synthesized iron oxide nanoparticles using *Grevillea robusta* Cunn. leaf extract against vector mosquitoes and their characterization. Experimental Parasitology 252:108586. <https://doi.org/10.1016/j.exppara.2023.108586>



The journal offers free, immediate, and unrestricted access to peer-reviewed research and scholarly work. Users are allowed to read, download, copy, distribute, print, search, or link to the full texts of the articles, or use them for any other lawful purpose, without asking prior permission from the publisher or the author.



**License** - Articles published in *Notulae Scientia Biologicae* are Open-Access, distributed under the terms and conditions of the Creative Commons Attribution (CC BY 4.0) License.

© Articles by the authors; Licensee SMTCT, Cluj-Napoca, Romania. The journal allows the author(s) to hold the copyright/to retain publishing rights without restriction.

**Notes:**

- **Material disclaimer:** The authors are fully responsible for their work and they hold sole responsibility for the articles published in the journal.
- **Maps and affiliations:** The publisher stay neutral with regard to jurisdictional claims in published maps and institutional affiliations.
- **Responsibilities:** The editors, editorial board and publisher do not assume any responsibility for the article's contents and for the authors' views expressed in their contributions. The statements and opinions published represent the views of the authors or persons to whom they are credited. Publication of research information does not constitute a recommendation or endorsement of products involved.